PERGAMON

International Journal of Heat and Mass Transfer 44 (2001) 1425–1438

International Journal of HEAT and MASS TRANSFER

www.elsevier.com/locate/ijhmt

A method for multiple steady line heat sources identification in a diffusive system: application to an experimental 2D problem

C. Le Niliot *, F. Lefèvre

Institut Universitaire des Systèmes, Thermiques Industriels, UMR CNRS 6595, Technopôle de Château Gombert, 5, Rue Enrico Fermi, 13 453 Marseille Cedex 13, France

Received 18 October 1999; received in revised form 30 March 2000

Abstract

This paper deals with an inverse problem which consists in the location identification of multiple-line heat sources placed in an homogeneous solid in the stationary case. The location and strength of the line heat sources are unknown. The identification procedure is based on the boundary integral formulation using Green functions. The discretized problem is non-linear if the location of the line heat sources is unknown. In order to solve the problem we use an iterative procedure to minimize a quadratic norm. The proposed numerical approach is applied to an experimental 2D example using measurements provided by an infrared scanner. The number of line heat sources is supposed to be known but we give some examples involving a number of sources superior or inferior to the real number.

1. Introduction

In this paper we propose an original method to cope with multiple-point heat sources identification when both intensity and location are unknown. As in the fundamental partial differential equation governing the heat transfer phenomena, the heat source generation is unknown, the problem is inverse and some additional information (measurements) are necessary to solve the problem.

In previous studies we have proposed a method to cope with this type of an inverse problem. In [1] we propose the Boundary Element Method (BEM) approach for point heat sources strength identification in diffusive systems when the location of the sources is known. The other authors working on the subject propose different methods such as adjoint method [2] or finite elements [3]. For all the proposed methods the location of the point heat sources is known, in [4] we propose an iterative algorithm for the case of a single source in a transient case.

In this paper we propose an iterative procedure for multiple heat source location in a diffusive system for the steady case. The formulation is based on a first-order approximation of the Green function used for BEM formulation. An iterative algorithm is built to minimize a cost function combining the boundary variables, measured or prescribed, and the modellized heat source contribution using a Green function [5].

The proposed method, valid for multiple sources identification, is applied on an academic experiment using infrared thermography. The aim is to avoid intrusive measurements but some thermocouples could be used. The experiment rather similar to the one presented in [4] is composed of a long square bar crossed by six heating wires, the aim is to identify the location and the strength of each activated wire without any a priori information. Some examples are proposed when the number of activated sources is unknown. The proposed inverse problem is ill posed in the sense of Hadamard [6] because the solution is not unique and as shown in the previous studies the strength of the source identification is highly sensitive to measurement errors. A simple regularization procedure is proposed in order to identify the strengths correctly.

* Corresponding author. Tel.: +33-04-9110-6886; fax: +33-04-9110-6969.

E-mail address: leniliot@iusti.univ-mrs.fr (C. Le Niliot).

0017-9310/01/$ - see front matter
PII: S0017-9310(00)00184-8

Nomenclature

A	linear system matrix
B	second member vector
c	multiplying coefficient
C	diagonal matrix
d	distance from the line heat source (mm)
g	heat source term (W m^{-3})
g	line heat source strength (W m^{-1})
h	heat transfer coefficient (W m^{-2} K^{-1})
H, **G**	matrices of stationary BIE
I	matrix for point source treatment
K	number of point sources
n	normal to the surface
N	boundary elements number
N'	internal points number
p	heat flux density (W m^{-2})
P	heat flux densities vector
q^*	normal derivative of T^*
S	source terms vector
t	time (s)
T	temperatures vector
T^*	fundamental solution
U	solution vector
x, y, z	Cartesian co-ordinates
X	x co-ordinates vector
Y	y co-ordinates vector

Greek symbols

δ	Dirac function
ε	emissivity
Γ	boundary of the diffusive domain
λ	conductivity (W m^{-1} K^{-1})
φ	measured heat flux density (W m^{-2})
θ	temperature in Celsius (°C)
Θ	vector of the heat sources contribution
σ	standard deviation
Ω	diffusive domain

Subscripts

k	point source index
∞	ambient conditions
c	convection

Superscripts

$'$	internal points
l	iteration number
$\hat{}$	least squares solution
$\sim$	approximated heat source contribution

Abbreviation

BEM	Boundary Element Method
BIE	Boundary Integral Equation

This paper is divided into two parts, the first one describes in detail the method used for the inverse problem resolution. We detail successively the BEM formulation for steady state conduction and the proposed inverse method. The second part describes the experiment and the results obtained in various conditions: one, two and four sources identification.

2. The point heat source identification

In this part of the paper we describe the BEM approach applied to the heat diffusion equation in the steady case. BEM is applied here in the sense of the point sources identification in the stationary case. The second part is related to the iterative algorithm used to identify the location of the sources.

2.1. The boundary element formulation for point heat sources location

The inverse method presented here is based on BEM and is already presented and detailed in [1] for point heat sources strength reconstruction. As it is pointed out in [1] the discretized boundary elements equations are not linear if the location of the heat sources is unknown. An iterative method is proposed in this section. In our problem the number of sources is supposed to be known.

2.1.1. The boundary integral equation

In terms of temperatures θ, the linear steady heat diffusion equation can be written:

$$\vec{\nabla}^2\theta + \frac{g}{\lambda} = 0, \tag{1}$$

where g is the heat source term, θ the temperature and λ is the heat conductivity.

Considering point M, of domain Ω of boundary Γ, integrating twice Eq. (1) weighted by a fundamental solution T^* [7], leads to the Boundary Integral Equation (BIE) for the linear stationary heat conduction. The linear BIE can be written:

$$c\theta_M + \int_\Gamma \theta q^* \,\mathrm{d}\Gamma = \int_\Gamma \frac{p}{\lambda} T^* \,\mathrm{d}\Gamma + \int_\Omega \frac{g}{\lambda} T^* \,\mathrm{d}\Omega, \tag{2}$$

where M is a point of Γ or Ω, p the heat flux density, T^* the fundamental solution, q^* the normal derivative of T^* and c a coefficient which depends on the position of M, namely $c = 1$, if M is in Ω and $c < 1$, if M is on Γ (e.g. $c = 0.5$ if Γ is smooth at M).

For non-linear thermal diffusion, the BIE formulation is possible using the Kirchoff transform [5] of the temperature as described in [7] and applied in [1]. The

fundamental solution T^* is a space-dependent Green function [5] which permits to cope with localized measurements (internal points) and singularities as point heat sources. The function T^* used to obtain Eq. (2) is a solution of

$$\Delta T^* + \delta_M = 0, \tag{3}$$

where δ_M is the Dirac function at point M of domain Ω. T^* is a Green function [5] which represents the response to a point heat source in an infinite domain, thus T^* can be written:

$$\text{in 2D } T^* = \frac{1}{2\pi}\ln\left(\frac{1}{r}\right), \tag{4}$$

$$\text{and in 3D } T^* = \frac{1}{4\pi}\frac{1}{r}, \tag{5}$$

where, in both cases, r is the distance between the current node and the point M of domain Ω. T^* is then the sensitivity coefficient to a strength variation of a point heat source placed at point M.

BIE (2) lets appear a volume integral related to heat source term g. In order to transform this volume integral into a discrete form without complete domain mesh, let us consider g as a set of K point heat sources as shown in [1,7].

Considering a set of line heat sources in a 2D diffusive system, by applying the explicit form of T^* the heat source term in BIE (3) can be written

$$\begin{aligned}\int_\Omega \frac{g}{\lambda}T^*\,\mathrm{d}\Omega &= \frac{1}{\lambda}\sum_{k=1}^{K}\mathrm{g}_k\frac{1}{2\pi}\ln\left(\frac{1}{r_k}\right)\\ &= \frac{1}{\lambda}\frac{-1}{4\pi}\sum_{k=1}^{K}\mathrm{g}_k\ln\left(\left((x_M-x_k)^2+(y_M-y_k)^2\right)\right),\end{aligned} \tag{6}$$

where g_k is the algebraic strength of source k, r_k the distance from considered point M to the source k, x_k (x_M) and y_k (y_M) the co-ordinates of line source k (point M).

The 3D case can be treated in a similar way, the problem in this case is to build a simple experiment with a point source in a 3D system.

2.1.2. The discrete formulation

It is important to notice that as it is mentioned in [1,7] using (6) in (2) leads to a boundary integrals only formulation. Thus to discretize domain Ω it is not necessary to build a complete domain mesh, a boundary discretization is sufficient to solve heat transfer Eq. (1).

As it is recommended in [7] and applied in [1], we use elements constant over space. This last assumption means that the temperatures and flux densities are taken to be constant on each element. Let us assume that the boundary Γ is discretized in N boundary nodes Γ_i. As a result, for an element Γ_i of the boundary we have

$$\begin{aligned}&\frac{1}{2}\theta_i + \sum_{j=1}^{N}\theta_j\int_{\Gamma_j} q^*\,\mathrm{d}\Gamma\\ &= \sum_{j=1}^{N}\frac{p_j}{\lambda}\int_{\Gamma_j}T^*\,\mathrm{d}\Gamma - \frac{1}{4\pi\lambda}\sum_{k=1}^{K}\mathrm{g}_k\ln\left(\left((x_i-x_k)^2+(y_i-y_k)^2\right)\right),\end{aligned} \tag{7}$$

where θ_i is the temperature at element Γ_i, p_i the heat flux density at element Γ_i, x_k and y_k the co-ordinates of line source k, x_i and y_i the co-ordinates of node i. In the latter equation we assume that the boundary is smooth at node i of the boundary. The integrals on the boundary elements Γ_j connect the ith node with the element Γ_j over which the integral is evaluated. Introducing coefficients $H_{i,j}$ and $G_{i,j}$, results of the above-mentioned integrals, we can build the following equation

$$\frac{1}{2}\theta_i + \sum_{j=1}^{N}H_{i,j}\theta_j = \sum_{j=1}^{N}\frac{G_{i,j}}{\lambda}p_j + \sum_{k=1}^{K}\frac{I_{i,k}}{\lambda}\mathrm{g}_k. \tag{8}$$

Coefficients $H_{i,j}$ and $G_{i,j}$ can be found in [7] and calculated analytically or numerically. $I_{i,k}$ is specific to heat source identification. Compared to the previous coefficients, coefficient $I_{i,k}$ is not the result of an integral but the value of the fundamental solution at node i considering the line source k.

Eq. (8) written for all the boundary nodes can be arranged in a matrix form and we obtain:

$$(\mathbf{C}+\mathbf{H})T = \mathbf{G}P + \mathbf{I}S, \tag{9}$$

where $\mathbf{C}$ is a diagonal matrix with 1/2 on the diagonal, $\mathbf{H}$ and $\mathbf{G}$ (N,N) dimension matrices of the coefficients $H_{i,j}$ and $G_{i,j}/\lambda$, T (P) the vector of temperatures (heat flux densities) at the boundary, $\mathbf{I}$ a (N, K) dimension matrix and S a (K) dimension vector containing the K unknown line heat sources intensities.

BIE (2) can be written for an internal point M and a discrete formulation using the above-mentioned assumptions leads to a matrix form with matrices $\mathbf{H}'$, $\mathbf{G}'$ and $\mathbf{I}'$ corresponding to the N' internal points, finally we obtain:

$$T' + \mathbf{H}'T = \mathbf{G}'P + \mathbf{I}'S, \tag{10}$$

where T' is the vector of the internal temperatures, $\mathbf{H}'$ and $\mathbf{G}'$ some matrices of (N', N) dimension and $\mathbf{I}'$ is a matrix of (N', K) dimension. As shown in [8,9] if the temperature at the internal points is known, for example a temperature measured by a thermocouple, system (9) can be combined with system (10). At least we obtain the final system

$$\begin{bmatrix}0\\ T'\end{bmatrix} + \begin{bmatrix}\mathbf{C}+\mathbf{H}\\ \mathbf{H}'\end{bmatrix}T = \begin{bmatrix}\mathbf{G}'\\ \mathbf{G}\end{bmatrix}P + \begin{bmatrix}\mathbf{I}\\ \mathbf{I}'\end{bmatrix}S$$

$$\text{or}\quad \begin{bmatrix}0\\ T'\end{bmatrix} + \begin{bmatrix}\mathbf{C}+\mathbf{H}\\ \mathbf{H}'\end{bmatrix}T - \begin{bmatrix}\mathbf{G}\\ \mathbf{G}'\end{bmatrix}P = \begin{bmatrix}\mathbf{I}\\ \mathbf{I}'\end{bmatrix}S. \tag{11}$$

System (11) contains $N+N'$ equations and $2N+3K$ unknowns, namely N boundary temperatures, N boundary heat flux densities, K point heat sources strengths and $2K$ co-ordinates ($3K$ in a 3D system). System (11) is used in the transient case [1] to identify unknown line heat sources intensities contained in vector S. In the present case, the location of point heat sources is unknown and system (11) is then non-linear.

If we have a set of boundary conditions, θ known, p known, $p=f(\theta)$ or both p and θ known, such as the number of unknowns is inferior to $N+N'$, the non-linear system (11) can be solved.

Let us introduce the vector Θ defined as the result of the following matrix operation:

$$\Theta=\begin{bmatrix}0\\T'\end{bmatrix}+\begin{bmatrix}\mathbf{C}+\mathbf{H}\\\mathbf{H}'\end{bmatrix}T-\begin{bmatrix}\mathbf{G}\\\mathbf{G}'\end{bmatrix}P \quad \text{with} \quad \begin{bmatrix}\mathbf{I}\\\mathbf{I}'\end{bmatrix}S=\Theta \tag{12}$$

Θ is an $(N+N')$ dimension vector. Vector Θ represents the contribution of the heat sources included in domain Ω. System (12) gives the beginning of our approach which consists in the comparison between the modelized contribution of heat sources and the measurements included in the right part of vector Θ.

The examples proposed in this paper consist in the complete knowledge of the boundary variables T and P, thus system (11) is reduced to the left-hand side equation. Nevertheless in most cases classical boundary conditions, Neumann, Dirichlet, Fourier, are applied on a portion of the boundary and matrix operation (12) cannot be performed readily. Vector Θ is evaluated into two steps. The first one is the resolution of system (11) using some prescribed co-ordinates and the second one is the resolution of system (12) using an iterative procedure in order to find out the location of the sources.

2.1.3. The point heat source intensity identification

For the point heat source intensity identification procedure, we use the same approach as the one presented in [1] for the transient case. When a priori location of the sources is known, it is possible to identify vector S components if the set of boundary conditions leads to a number of M unknowns (K sources and $M-K$ boundary conditions) inferior to or equal to the number of equations $(N+N')$.

If we rearrange system (11) and combine the unknowns in a vector U, we obtain:

$$\mathbf{A}U=B, \tag{13}$$

where $\mathbf{A}$ is a matrix of dimension $((N+N'),\ \mathrm{M})$, U a vector of dimension (M) and B is a second member vector of dimension $(N+N')$. In the general case we have more measurements than unknowns $(N+N'>M)$ and vector U has to minimize a cost function $J(U)$ defined as:

$$J(U)=\|\mathbf{A}U-B\|^2. \tag{14}$$

In order to find a solution to the inverse problem we have to solve the following optimization problem:

$$\hat{U}=\arg(\min(J(U))). \tag{15}$$

If we apply the least squares method (in the case of an Euclidean norm) to minimize function (14), this leads to a vector $\hat{U}$ solution in the sense of the least squares. As a result $\hat{U}$ is the solution of the simultaneous equations:

$$(\mathbf{A}^{\mathbf{T}}\mathbf{A})\hat{U}=\mathbf{A}^{\mathbf{T}}B \tag{16}$$

with the components of $\hat{U}$ identified using a least squares minimization we obtain the complete knowledge of the boundary variables θ and p assembled in vectors $\hat{T}$ and $\hat{P}$. The latter contain measurements and identified values. In vector $\hat{S}$ we find the values of the heat sources strength extracted from vector $\hat{U}$.

As shown by Beck et al. [10] the inverse heat conduction problem is ill posed considering the stability of the solution to measurement errors. Thus the result of system (16) can be unstable considering the measurement errors and the heat sources location errors. In our case it is not possible to use a space regularization procedure because of the singular character of point heat sources. Considering the reduced number of sources and the a priori information that the strength is positive, the identified strength of each source is normalized considering that a source cannot be negative and that the sum of the sources is equal to the total boundary heat flux.

2.1.4. The cost function for location identification

Using the least squares approach it is possible to compare the space-dependent heat source contribution vector and the boundary and internal measurement vector such as defined in Eq. (12). Let us introduce two vectors $\hat{\Theta}$ and $\tilde{\Theta}$, whose expressions are:

$$\hat{\Theta}=\begin{bmatrix}0\\T'\end{bmatrix}+\begin{bmatrix}\mathbf{C}+\mathbf{H}\\\mathbf{H}'\end{bmatrix}\hat{T}-\begin{bmatrix}\mathbf{G}\\\mathbf{G}'\end{bmatrix}\hat{P} \tag{17}$$

and

$$\tilde{\Theta}=\begin{bmatrix}\tilde{\mathbf{I}}\\\tilde{\mathbf{I}}'\end{bmatrix}\hat{S} \tag{18}$$

In the latter equations $\hat{}$ denotes the least squares solution obtained from Eq. (16) and $\sim$ denotes the heat sources location-dependent vector. Using exact

strength and exact location we have: $\tilde{\Theta} = \hat{\Theta}$. Using an inverse approach, where the location and the strength of the sources are unknown, the aim is to minimize the distance between vectors $\hat{\Theta}$ and $\tilde{\Theta}$. Vector $\tilde{\Theta}$ is calculated using some approximated locations contained in matrices $\tilde{\mathbf{I}}$ and $\tilde{\mathbf{I}}'$ and the vector of the identified strengths $\hat{S}$.

An iterative algorithm must be performed to minimize the distance between vector $\hat{\Theta}$ and vector $\tilde{\Theta}$. For location identification, the aim is to find out vectors X and Y, vectors of the x and y co-ordinates of the sources. As a result the co-ordinates included in X and Y are solutions of:

$$(X, Y) = \arg\{\min \|\hat{\Theta} - \tilde{\Theta}\|^2\}, \tag{19}$$

where $\hat{\Theta}$ and $\tilde{\Theta}$ vectors calculated as specified in Eqs. (17) and (18).

The proposed method can be decomposed into two steps, the first one consists in the identification of $\hat{S}$, $\hat{T}$ and $\hat{P}$ using some specified locations. The second one is a first-order approximation of matrices $\mathbf{I}$ for location identification. The two steps are included in an iterative process. The following sections focus on the iterative algorithm performed to locate the sources.

2.2. The iterative algorithm for the point heat source location

In this part of the paper we describe the method used to solve the non-linear problem (19). The method used is a Newton method using the first term of the Taylor development of the Green function. In the second part of this paragraph we describe the complete procedure connecting the strength and boundary variables identification and the location identification procedures. It has to be noticed that all the developments presented are given for the 2D case. The 3D case is similar and it can be performed readily using the form of T^* given in Eq. (5).

2.2.1. The iterative method

The aim is to find the co-ordinates of the heat sources using an iterative procedure. As we can see in Eq. (6), components of matrices $\tilde{\mathbf{I}}$ and $\tilde{\mathbf{I}}'$ are non-linear in x_k and y_k, the 2D co-ordinates of line heat source k. In this section we propose a classical non-linear method to solve (19), the method is based on the first term of the Taylor development of coefficients $I_{i,k}$ described in Eq. (6). The strengths g_k identification procedure is not included in the development. The strengths used in the first-order approximation are found by solving system (16) at iteration l.

Let us take source k considering boundary node Γ_i (or internal point i) of co-ordinates x_i and y_i, at iteration $l+1$, in the 2D case the first-order term of the Taylor development can be written

$$\begin{aligned}
&\frac{-1}{4\pi} \ln\left(\left((x_k^{l+1} - x_i)^2 + (y_k^{l+1} - y_i)^2\right)\right) g_k^l \\
&\quad \approx \frac{-1}{4\pi} \ln\left(\left((x_k^{l} - x_i)^2 + (y_k^{l} - y_i)^2\right)\right) g_k^l \\
&\quad - \frac{1}{4\pi} \frac{2(x_k^l - x_i)}{(x_k^l - x_i)^2 + (y_k^l - y_i)^2} g_k^l \Delta x_k^{l+1} \\
&\quad - \frac{1}{4\pi} \frac{2(y_k^l - y_i)}{(x_k^l - x_i)^2 + (y_k^l - y_i)^2} g_k^l \Delta y_k^{l+1},
\end{aligned} \tag{20}$$

where $\Delta x_k^{l+1} = x_k^{l+1} - x_k^l$ and $\Delta y_k^{l+1} = y_k^{l+1} - y_k^l$. In Eq. (20) exponent l denotes, for the concerned variables, the iteration dependence.

Using a first-order assumption leads to a linear system considering heat sources location at iteration l and Δx_k^{l+1}, Δy_k^{l+1} the errors on source k location at iteration $l+1$. Let us introduce the dimension K vectors ΔX^{l+1} and ΔY^{l+1} whose components are respectively, Δx_k^{l+1} and Δy_k^{l+1}. Introducing Eq. (20) for the whole boundary nodes leads to the linear system

$$\hat{\Theta}^l - \tilde{\Theta}^l = \begin{bmatrix} \mathbf{E}^l \\ \mathbf{E}'^l \end{bmatrix} \Delta X^{l+1} + \begin{bmatrix} \mathbf{D}^l \\ \mathbf{D}'^l \end{bmatrix} \Delta Y^{l+1}, \tag{21}$$

where $\hat{\Theta}^l$ is the result of matrix operation (17), $\tilde{\Theta}^l$ the vector of calculated heat sources term calculated at iteration l (see Eq. (18)), ΔX^{l+1} and ΔY^{l+1} vectors of components Δx_k^{l+1} and $\Delta y_k^{l+1} (1 \leqslant k \leqslant K)$ at iteration $l+1$. Matrices $\mathbf{D}^l$ and $\mathbf{E}^l$ are (N, K) dimension matrices, a result of the first derivative components of $\mathbf{I}^l$ for each variable. At iteration l and node Γ_i, or internal point i, the source k components of matrices $\mathbf{D}^l$, $\mathbf{E}^l$ are:

$$\begin{aligned}
[\mathbf{D}^l]_{i,k} &= \frac{-1}{4\pi\lambda} \frac{2(x_k^l - x_i)}{(x_k^l - x_i)^2 + (y_k^l - y_i)^2} g_k^l, \\
[\mathbf{E}^l]_{i,k} &= \frac{-1}{4\pi\lambda} \frac{2(y_k^l - y_i)}{(x_k^l - x_i)^2 + (y_k^l - y_i)^2} g_k^l.
\end{aligned} \tag{22}$$

2.2.2. The iterative algorithm

In this section we present the iterative procedure used to locate the point heat sources. This procedure uses alternately the least squares estimation of the strengths vector and the first-order approximation of the error described in the previous paragraph. The iterative procedure begins with an a priori (initial) location for each source.

At iteration l, the first step is the inverse problem resolution represented by system (16), the strengths are identified using the locations (x_k^l, y_k^l) $(1 \leqslant k \leqslant K)$. The inverse problem resolution is followed by a resolution of system (21), which is the second step. The new co-ordinates of the sources are calculated such as

$$x_k^{l+1} = x_k^l + \Delta x_k^{l+1}, \quad y_k^{l+1} = y_k^l + \Delta y_k^{l+1}$$

and used to solve the inverse problem described by Eq. (16) at iteration $l+1$. At the end of the algorithm the co-ordinates converge on the sources location with the correct strength. As the inverse problem is unstable considering the errors on the co-ordinates Δx_k^{l+1} and Δy_k^{l+1}, the latter are controlled in order to avoid an intermediate location (x_k^{l+1}, y_k^{l+1}) out of the domain. The direction given by the successive locations at iterations l and $l+1$ is preserved but the maximum distance covered between two successive locations $(\sqrt{(\Delta x_k^{l+1})^2 + (\Delta y_k^{l+1})^2})$ is imposed at 1/5 of Ω characteristic dimension. This procedure reduces the excursions of the sources out of the domain, thus the number of iterations is reduced. Nevertheless if during the iterative process a location is found out of the domain, a new location is randomly imposed in the domain.

Of course the a priori locations are important in order to converge as rapidly as possible, i.e. the error on the co-ordinates has to be reduced. In order to reduce the path length of the source from its initial location to its final destination, the locations at iteration $l = 0$ are chosen at the centre of the diffusive system. All these locations are slightly different in order to avoid a singular matrix $\mathbf{A}$. Actually, if all the line sources are at the same location, the equations constituting matrix $\mathbf{A}$ are degenerated. A consequence is that all the heat source strengths obtained from system (13) are identical and the correct co-ordinates cannot be determined.

The stopping criteria are based on co-ordinates variations between two iterations, in our examples we use 0.15 mm: the radius of the experimental sources. Another stopping criterion can be introduced by calculating the norm $\|\hat{\Theta}^l - \tilde{\Theta}^l\|$ at each iteration, the evolution of this norm is interesting to evaluate the capability of the process to converge. If $\|\hat{\Theta}^l - \tilde{\Theta}^l\|$ is constant it means that the minimum is obtained according to the proposed method, then the iterative process has to be stopped. A convergence study is presented in the following section, the algorithm is applied to our experiment using different initial locations.

A third stopping criterion could be introduced by calculating the norm $\|T_{\text{mes}} - \hat{T}\|$ where vector $\hat{T}$ contains the calculated temperatures using the results of the inverse problem and a direct BEM approach. These calculated temperatures are compared to the vector of the measurements T_{mes}. The use of this criterion imposes the resolution of the direct problem at each iteration which is not our aim.

In order to test our approach, rather than a numerical experiment we have chosen to present some experimental results which is the scope of the following section.

3. A 2D experiment using infrared thermography

The experimental design is a long square bar crossed in its longest dimension by multiple, in fact six, thin heating wires (0.3 mm diameter). Each heating wire represents a point heat source. The proposed experimental set-up is very similar to the set-up proposed in [4]. The chosen material is cement which leads to a good resistance to fracture at the temperature reached in our experiment.

Our approach for solving inverse problems has to be implemented with the thermal conductivity λ because with this type of material the thermal conductivity λ depends on many factors. A parameter identification is performed "in situ" on the experiment using a particular set of sensors and the central heating wire.

In the presented examples all the boundary variables, i.e. heat flux densities and temperatures, are known along the entire diffusive system boundary. This particular boundary condition is obtained associating the measured temperature field with the calculated heat transfer coefficient. Thus as vectors $\hat{T}$ and $\hat{P}$ are known, vector $\hat{\Theta}$ can be calculated readily using Eq. (17).

Such restrictive boundary conditions are not essential to solve the inverse problem. Some other boundary conditions can be applied on a part of the domain, i.e. Neumann, Fourier or Dirichlet if the measurements are in a sufficient number to permit the inverse problem resolution. The measurements can be obtained for instance from internal sensors.

3.1. The experimental design

The experimental design under investigation is a long square section bar of cement crossed in its longest dimension by six KANTHAL® heating wires of 0.3 mm diameter. In the central section of the bar, the diffusion system is assumed to be bidimensional. Considering the heating wires diameter (0.3 mm) compared to the section of the bar $(50 \times 50\ \text{mm}^2)$, the heat generation can be approximated by a point in a section. The KANTHAL® wires are heated by Joule effect. The current is imposed by some DC power supplies. If we call L the length of the heating wire, the imposed strength of the source is: $g = \text{current} \times \text{voltage}/L$.

The bar is fixed vertically on a rotating deck screwed onto an optical bench (cf. Fig. 1). The infrared scanner, an AGEMA® 880 LW, is placed on the same bench. This system permits to scan each boundary without changing the focus by rotating the deck. All the surfaces are painted in black. The black paint emissivity ε is 0.95, in the wavelength range of the scanner: 8–12 μm.

In the section under investigation two sensors can be found at the positions displayed in Fig. 2. The two sensors tc1 and tc2 are placed at 10 mm from the central source $g6$. They are used to identify the heat conduc-

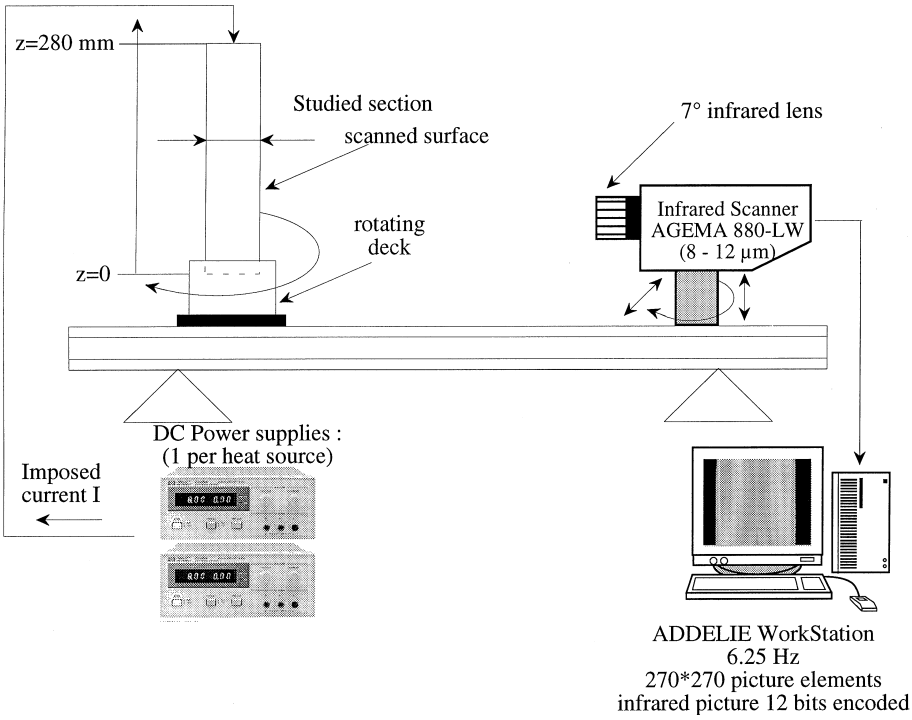

Fig. 1. The experimental set-up scheme.

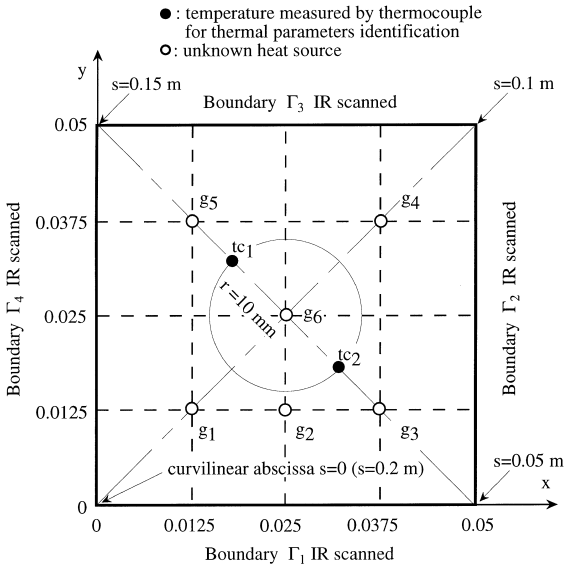

Fig. 2. Sensors location and boundary conditions in the studied section.

tivity of the material using a method similar to the two-linear probe method proposed in [11].

The surface temperature is measured using an infrared scanner AGEMA® 880 LW. The infrared pictures constituted of 270×270 pixels (picture elements) are hard disc-recorded using software ADDELIE© (ADDITIONNAL TECHNOLOGIES). In the steady case, 100 pictures are averaged in order to decrease the measurement errors. Using a calibration equation it is possible to obtain the surface temperature. The infrared scanner is calibrated at the laboratory using the procedures described in [12]. In the range 30–120°C, using the calibration equation leads to the largest error of 0.08 K, a null mean error and a standard deviation of 0.06 K.

In the obtained infrared picture used as a data-file it is necessary to extract 25 values representing the 25 boundary elements over each side of the bar. To obtain this information from the picture we use a quadratic interpolation over the concerned pixels and the average temperature is then calculated at the middle of the element.

The section at $z = 180$ mm is our 2D diffusive system, this section is described in Fig. 2. In the latter we find six different sources, from $g1$ to $g6$, and two thermocouple junctions. The six heating wires are independent and can be activated separately with different currents. A maximum of four heating wires are activated at the same time.

3.2. The experimental inverse problem

In this paragraph we present the boundary conditions associated with the measurements used to solve

the inverse problem. The 2D section under investigation is discretized in 100 BEM linear elements. The inverse problem consists in identifying each activated heat source location and the associated strength. To cope with this problem we use the following boundary conditions:

- Γ_1–Γ_4: known temperatures (measurements from infrared thermography).
- Γ_1–Γ_4: known heat flux density.

The heat flux densities over the scanned surfaces are obtained as the sum of radiant and convective losses. For the radiant heat flux density we have: $\varphi_r = \varepsilon\sigma(T_r^4 - T_i^4)$ with T_r the radiant ambient temperature in Kelvin and T_i the measured temperature at element Γ_i of the scanned boundary. For the convective heat transfer coefficient h_c we use the local relations along z axis proposed in [13] for a vertical cylinder in calm air. This correlation is used considering an average temperature along s but as a function of z because of the vertical position of the bar. In Figs. 3 and 4, we present some results obtained for an intensity of 40 W m^{-1} on $g6$, a radiant ambient temperature of 25°C and an air temperature of 25°C. In Fig. 3, we show the average boundary temperature function of z. As we can see on this chart the average boundary temperature is a function of z. The studied section is situated at $z = 0.18$ m, in this region the temperature variations are smooth and a linear approximation leads to a gradient of 7°C/m.

Using the average temperature function of z T_z, it is possible to obtain a measured heat transfer coefficient by convection. The latter is obtained using the following equation:

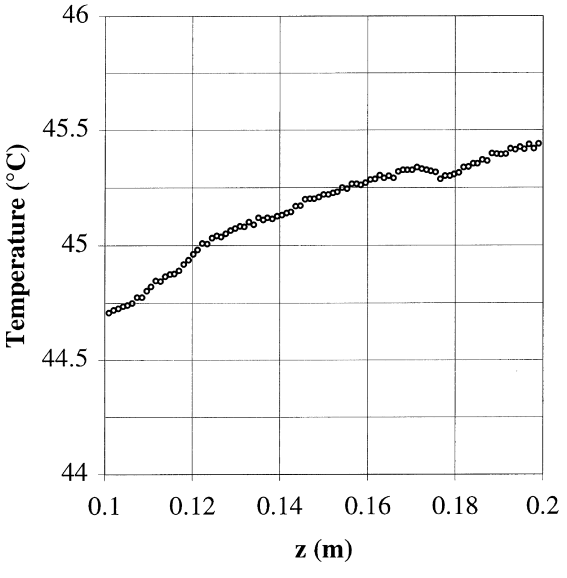

Fig. 3. Mean boundary temperature evolution along z for steady state, $g6 = 40$ W m^{-1}, $\theta_\infty = 25$°C.

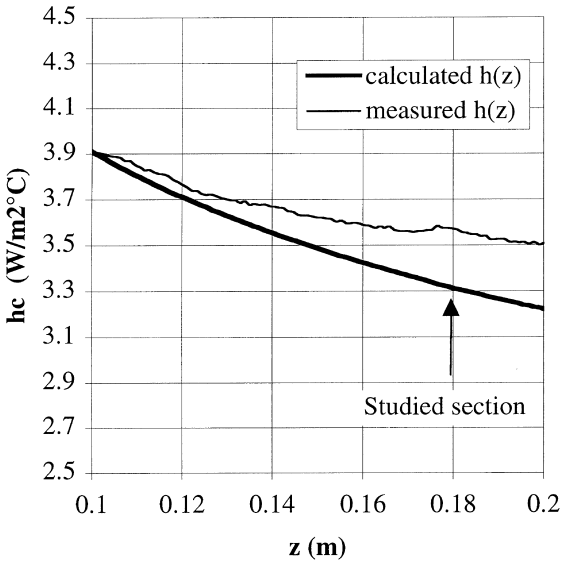

Fig. 4. Convective heat transfer coefficient h_c on the scanned boundary, calculated and measured.

$$h_c(z) = \frac{\varphi - \sum_{i=1}^{25} \varepsilon\sigma(T_r^4 - T_i^4)}{(T_\infty - T_z)}, \tag{23}$$

where T_z is the average side temperature along z, φ the average heat flux density imposed by the central heating wire $g6$ (here 200 W m^{-2}), and T_i the temperature measured on element Λ_i, $1 \leqslant i \leqslant 25$ on one side.

In Fig. 4 we have plotted the measured convection heat transfer coefficient and the one obtained using the correlation. We obtain some satisfactory results between $z = 0.1$ m and $z = 0.2$ m. In the studied section we obtain 3.56 W m^{-2} K^{-1} for the measured coefficient and 3.31 W m^{-2} K^{-1} for the calculated coefficient using the correlation. This corresponds to an error of 7.5% on the calculated heat flux density by convection (65.6 W m^{-2}). Let us remind that the total heat flux density here is of 200 W m^{-2}. Including the radiant flux density we obtain for this particular case a value for the calculated heat flux density of 194.9 W m^{-2} which represents a total deviation of 2.6%. A sensitivity study on the calculated convection heat transfer coefficient is given in the following sections.

In the latter the heat flux densities obtained using the measured temperature profile along the studied section is calculated for each element. A local relation is used for the radiant heat flux density and the calculated coefficient $h_c(z)$ is applied on each element. Including radiant and convective losses, the measured heat flux density φ_i at boundary element Γ_i associated with the measured temperature T_i is given by the relation:

$$\varphi_i = \varepsilon\sigma(T_r^4 - T_i^4) + h_c(z)(T_\infty - T_i), \tag{24}$$

where $h_c(z)$ is the convective heat transfer coefficient in W m^{-2} °C^{-1} evaluated at $z = 0.18$ m using the average boundary temperature at the studied section.

The thermal profile displayed in Fig. 3 shows that due to a variation of the heat transfer coefficient along z axis the diffusive system is not strictly 2D. Considering the temperature function of z around the studied section from $z = 0.1$ m to $z = 0.2$ m, a linear approximation leads to a gradient of: $\partial T/\partial z = 7$°C/m. This gradient is the same at the surface and inside the bar, this last assumption has been verified through direct simulations. The minimum value of $\partial T/\partial n$ calculated by direct simulations is around −264°C/m, it can be along x or y depending on the considered area. The maximum ratio between the gradients in the plan (x, y) and the gradient along z is 2.6%. This low value can justify a 2D approximation.

3.3. The experimental results

This paragraph presents some results obtained for the square bar, in most examples we use the exact number of sources activated but for some examples we will consider more or less heat sources than really activated. For these cases the solution can be not unique depending on the initial position. The results are displayed in tables giving the expected and identified values with some additional information as:

- the value of the Euclidean norm $\|\hat{\Theta} - \tilde{\Theta}\|$ in °C;
- the value of the standard deviation

$$\sigma(\theta) = \sqrt{\frac{\sum_{i=1}^{N}\left(\theta_{i,\text{measured}} - \hat{\theta}_{i,\text{calculated}}\right)^2}{N}} \text{ in °C.}$$

Norm $\|\hat{\Theta} - \tilde{\Theta}\|$ represents the distance between the heat source term modellized (cf. Eq. (18)) and the least squares estimation of Θ (cf. Eq. (17)). $\sigma(\theta)$ is the standard deviation between the results of a direct problem and the measured temperatures. These two criteria are interesting to compare the different results. As it is mentioned in Section 2, $\|\hat{\Theta} - \tilde{\Theta}\|$ is calculated during the iterative process which is not the case with $\sigma(\theta)$, a result of the comparison between the measured temperatures and the calculated temperatures. The latter are obtained from the resolution of a direct problem using the identified locations and strengths.

3.3.1. The number of sources is correct

The first example concerns a single source activated, in Table 1 we present three different identifications corresponding to three sources activated separately with a strength of 40 W m^{-1}. The presented results are the errors Δx and Δy, respectively on the x and y co-ordinates. They are calculated such as $\Delta x = x_{\text{experimental}} - x_{\text{identified}}$. Parameter d, given in mm, is the distance between the identified and experimental source ($d = \sqrt{\Delta x^2 + \Delta y^2}$). As we can see in Table 1 the location identification is accurate with a maximum distance between the identified and experimental source of 1.1 mm. The results are also good for the strength identification, the maximum deviation is −1.4 W m^{-1}: 3.5% of the experimental strength. These satisfactory results show that the model is relevant concerning the heat flux density field associated with the measured temperature field on the scanned surface.

In Table 2 we present the results obtained for some cases where two sources are simultaneously activated. As for the single source the results can be considered satisfactory, nevertheless the location error d is now of 1.6 mm compared to the 1.1 mm of the previous examples. The error on the strength is raised to 8.9% on $g3$ intensity. With two sources at 30 W m^{-1} the surface temperature increases and the assumption of a global convective heat transfer coefficient might not be valid.

For the last example of this section we propose to identify simultaneously four different sources, the four sources located at the four corners. The four intensities are different from 10 to 40 W m^{-1}. This case is difficult because the sensitivity to the position is very low with a strength of 10 W m^{-1}. The results of the identification are presented in Table 3. These results are good when the strength of the concerned source is over 20 W m^{-1} which is not the case with $g1$. Even with this poor estimation of $g1$ the other sources are well identified. The value of the standard deviation $\sigma(\theta)$ is 0.22°C and as we can see in Fig. 5 the temperature profiles, measured and calculated, are very close. The main differences are noted at the boundaries of each side, at curvilinear abscissa s equal to 0.05, 0.1, 0.15 and 0.2 m. This lack of accuracy

Table 1
Results of three identifications involving a single source: $g1$, $g2$ or $g6$

Source	Strength g (W m^{-1})	d (mm)	Δx (mm)	Δy (mm)	Δg (W m^{-1})	$\|\hat{\Theta} - \tilde{\Theta}\|$ (°C)	$\sigma(\theta)$ (°C)
$g1$	40	1.1	0.9	0.7	−0.9	0.74	0.14
$g2$	40	0.6	−0.5	0.4	−1.1	0.95	0.14
$g6$	40	0.3	−0.3	0.1	−1.4	0.78	0.15

Table 2
Results of two identifications involving two sources: $(g1, g3)$ or $(g3, g5)$

Source	Strength g (W m^{-1})	d (mm)	Δx (mm)	Δy (mm)	Δg (W m^{-1})	$\|\hat{\Theta} - \tilde{\Theta}\|$ (°C)	$\sigma(\theta)$ (°C)
Identification of g3 and g5							
$g1$	30	0.3	0.3	0.1	−0.4	1.02	0.18
$g3$	30	1.6	1.6	0	−2.7		
Identification of g3 and g5							
$g3$	30	0.8	0.8	−0.2	−2.4	1.06	0.17
$g5$	40	1.1	0.6	−0.9	−1.8		

Table 3
Results of an identification involving four sources: $g1$, $g3$, $g4$ and $g5$

Source	Strength g (W m^{-1})	d (mm)	Δx (mm)	Δy (mm)	Δg (W m^{-1})	$\|\hat{\Theta} - \tilde{\Theta}\|$ (°C)	$\sigma(\theta)$ (°C)
$g1$	10	3.5	−0.6	−3.5	0.0	1.58	0.22
$g3$	20	1.9	1.9	0.3	2.3		
$g4$	30	1.4	0.1	1.4	−3.5		
$g5$	40	0.4	−0.4	−0.1	−1.4		

is a consequence of an imperfect focus of the infrared scanner around the boundaries of the scanned object.

3.3.2. Influence of the initial location

Through an example we propose to examine the influence of the initial location on the results of the identification procedure. Let us examine the above-mentioned case with sources $g3$ and $g5$ activated. The previous identification has been performed using the initial locations at the centre of the bar, at two different locations at 0.1 mm of the centre. The results after four iterations are given in Table 2. In order to test the stability of the results to initial locations the path covered by the identified locations during the iterative process is recorded. The results are displayed in Fig. 6 for four different initial locations: at the corners, at the centre ... The number of iterations necessary to respect the stopping criterion is given in each figure. The stopping criterion here is of 0.15 mm which corresponds to the radius of the heating wires. All the obtained final locations are the same within 0.1 mm. The path followed by the sources is continuous for cases (a)–(c) with an iteration number inferior to six. The path followed by the sources in case (d) is not continuous like the others and the number of iterations necessary to converge is higher (11 iterations). This can be explained by an ill conditioned resolution matrix due to the location of both sources at the centre of the bar. At this point of the process if the space step between two iterations is not controlled the point sources would be located out of the domain. The same comment can be made for the example displayed in Fig. 6(a) at the beginning of the iterative process.

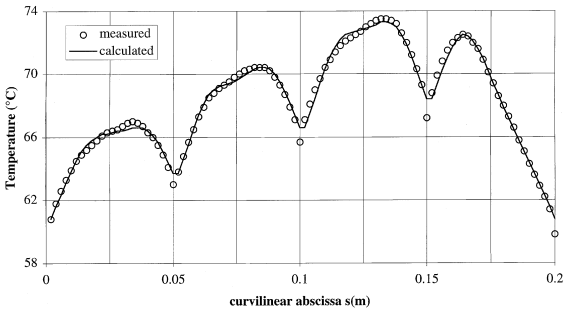

Fig. 5. Temperatures (°C) measured and calculated at the scanned surface using the results given in Table 3 with the four identified sources.

In Fig. 7, we present the variation of the Euclidean norm during the iterative process performed in case (c) described in Fig. 6. As we can see, the shape of the function is continuous by decreasing, which validates the iterative method in this particular case.

Concerning the above-mentioned examples, the results obtained are not a function of the initial locations. The same results are obtained within the stopping criterion (here 0.15 mm) whatever the chosen initial locations. This is not the case when the number of activated sources is not correct. An other parameter is important for a correct strength identification: the calculated heat transfer coefficient.

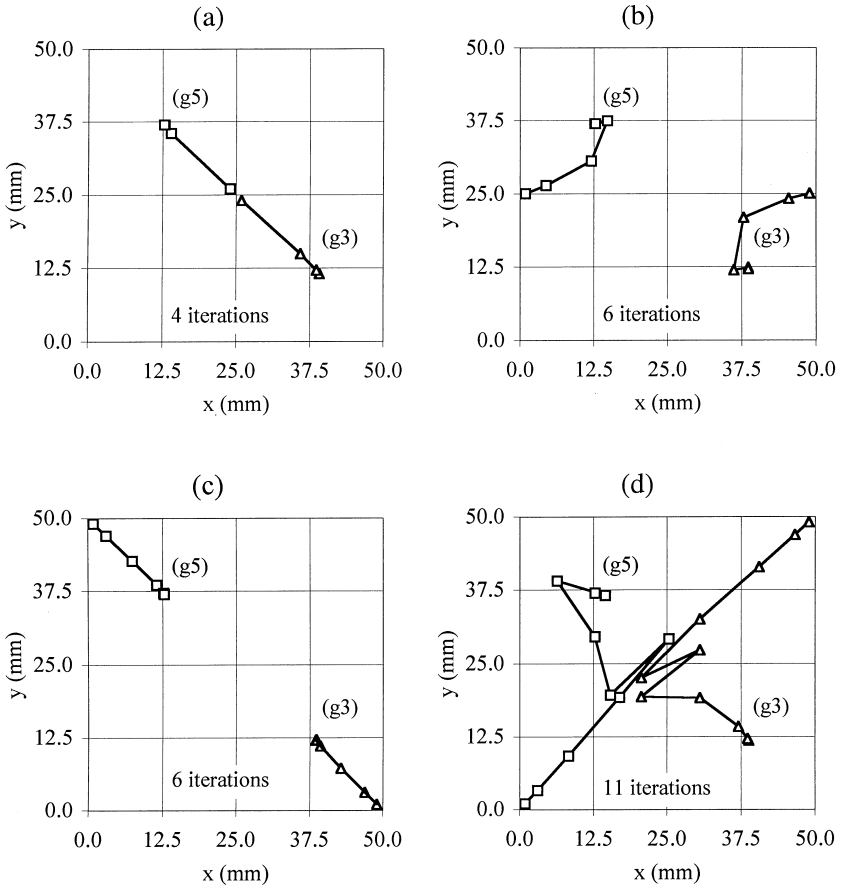

Fig. 6. Path followed by the searched heat sources ($g3$ and $g5$) during the iterative process for different initial locations: (a) $g3(25.1;24.9)$ $g5(24.9;25.1)$, (b) $g3(1;25)$ $g5(49;25)$, (c) $g3(49;1)$ $g5(1;49)$ and (d) $g3(1;1)$ $g5(49;49)$.

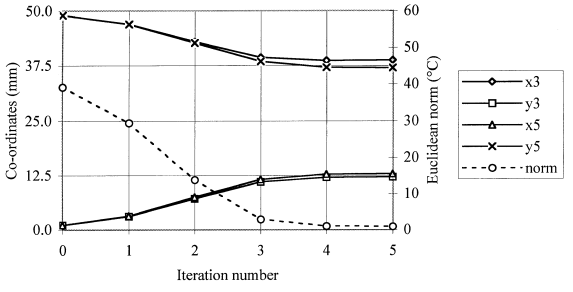

Fig. 7. $g3$ and $g5$ co-ordinates and $\|\hat{\Theta} - \tilde{\Theta}\|$ (norm) versus the iteration number, during the iterative process with initial locations $g3(49;1)$ and $g5(1;49)$.

3.3.3. Influence of the calculated convective heat transfer coefficient

In this section, we propose to study the sensitivity of the result to convective heat transfer coefficient h_c. Let us consider the four activated sources example presented in Table 3. In the latter the results are obtained with the calculated value: $h_c = 4.0\ \mathrm{W\ m^{-2}\ K^{-1}}$. Let us perform an identification with heat transfer coefficient $h_c \pm 10\%$; the results are given in Table 4.

In this table we can see that a variation of 10% on the calculated heat transfer coefficient h_c does not lead to a variation of 10% on the error. Compared to the results given in Table 3, the identified value of the source is increased, or decreased, of about 8% in the worse case ($g1$). A deviation of 2% is observed in the best case ($g5$). About the total energy reconstruction we have a sum of the errors Δg equal to $-6.0\ \mathrm{W\ m^{-1}}$ for $h_c - 10\%$ and $+0.8\ \mathrm{W\ m^{-1}}$ for $h_c + 10\%$. These values represent, respectively, -6% and 0.8% of the total strength imposed by the four sources. These results let appear a bias on the effective value of calculated coefficient h_c, but in a satisfactory range especially for location identification. This is the cost for using measured boundary variables only and particularly measured heat flux densities through a calculated heat transfer coefficient.

In the next paragraph we examine the case of an unknown number of sources, in this case we try to

Table 4
Results of identifications involving four sources: $g1$, $g3$, $g4$ and $g5$ with the calculated convective heat transfer coefficient $h_c \pm 10\%$

Source	Strength g (W m^{-1})	Distance d (mm)		Δg (W m^{-1})	
		$h_c - 10\%$	$h_c + 10\%$	$h_c - 10\%$	$h_c + 10\%$
$g1$	10	3.6	3.5	−0.7	0.8
$g3$	20	1.9	1.9	1.5	3.1
$g4$	30	1.3	1.4	−4.5	−2.6
$g5$	40	0.4	0.4	−2.3	−0.5

identify more or less sources than present in the domain, which can lead to not unique solutions depending on the a priori locations used to initialise the iterative process.

3.3.4. The number of heat sources is unknown

In this paragraph, we present some identification results for the case where the number of point heat sources is unknown which can lead to declare more or less sources than expected. The results are presented using a scheme of the studied section. The plain symbols (● and ■) correspond to the real sources, the white symbols (○ and □) correspond to the identified sources. The intensities are indicated in (W m^{-1}) and are represented between brackets beside each concerned source. When an identified source is not close enough to a real source it is indicated by symbol "+".

In Fig. 8 we have represented the results for one source activated and four declared. As we can see, the result of the identification corresponds to the result of Table 2 for one source declared. Indeed, one of the declared sources corresponds to the real source $g2$ with a similar strength and a similar location, the strength of the three others is nearly equal to zero.

In Figs. 9–11 we present the cases of sources $g1$ and $g3$ activated using a number of declared sources, different for two. In Fig. 9, only one source is declared. As it could be predicted, at the end of the iterative process, the identified source takes place between $g1$ and $g3$. The found intensity is very close to the sum of the intensities of $g1$ and $g3$. The proposed number of sources can be eliminated considering the value of the standard deviation (1.9°C) or the value of the Euclidean norm (9.2°C). The latter are ten times higher than those calculated in the case where two or more sources are declared.

In Figs. 10 and 11 we show the same case with respectively, 3 and 4 sources declared. The results are similar to the example presented in Fig. 8. Two of the

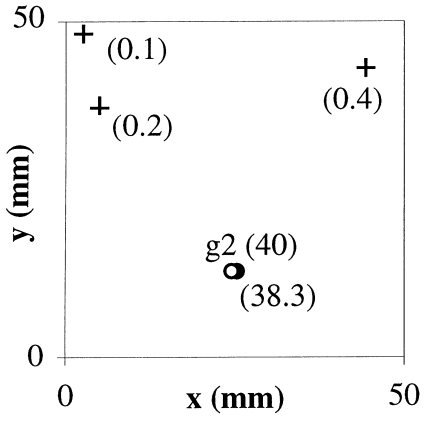

Fig. 8. One source activated $g2$, four declared, $\|\hat{\Theta} - \tilde{\Theta}\| = 0.86$°C, $\sigma(\theta) = 0.11$°C.

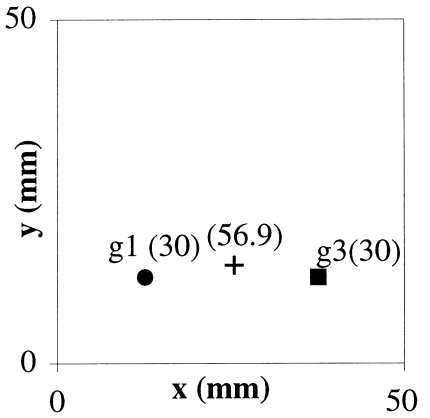

Fig. 9. Two sources activated, $g1$ and $g3$, one declared, $\|\hat{\Theta} - \tilde{\Theta}\| = 9.19$°C, $\sigma(\theta) = 1.93$°C.

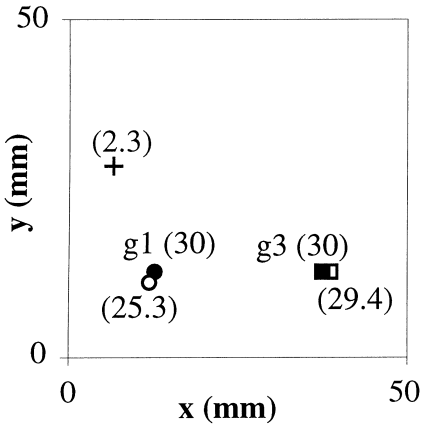

Fig. 10. Two sources activated, $g1$ and $g3$, three declared, $\|\hat{\Theta} - \tilde{\Theta}\| = 0.84$°C, $\sigma(\theta) = 0.15$°C.

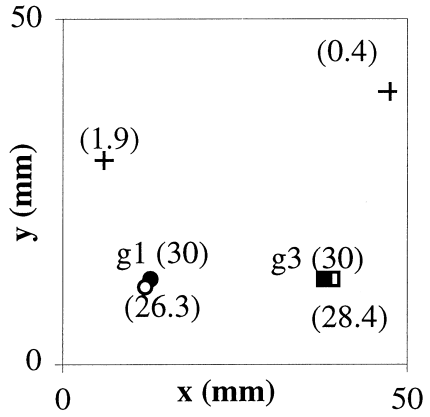

Fig. 11. Two sources activated, $g1$ and $g3$, four declared, $\|\hat{\Theta} - \tilde{\Theta}\| = 0.77°C$, $\sigma(\theta) = 0.13°C$.

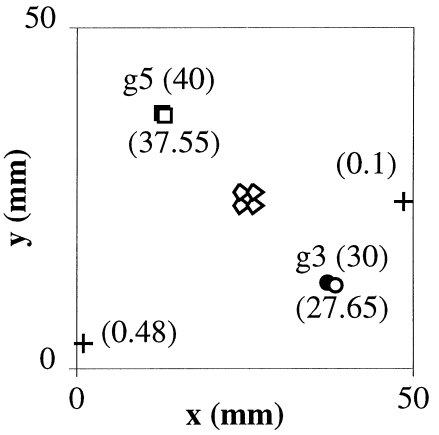

Fig. 13. Two sources activated, $g3$ and $g5$, four declared, initial locations at the centre (◇), $\|\hat{\Theta} - \tilde{\Theta}\| = 0.94°C$, $\sigma(\theta) = 0.13°C$.

declared sources correspond to the real sources $g1$ and $g3$, the strength of the others, indicated by symbol "+", are at least 10 times smaller than these ones. The values of standard deviation and Euclidean norms are of the same order of magnitude as those calculated when two sources are declared (see Table 3). These values are a little smaller when the number of declared sources is more important, which can be explained considering that the supplementary sources, with a very low intensity, adjust to the measurements and modelling errors.

The results presented in Figs. 12 and 13 show two different solutions of the identification problem of two sources $g3$ and $g5$ when four sources are declared. These results are obtained using different initial conditions; at the four corners for the results displayed in Fig. 12 and in the centre for the results displayed in Fig. 13. As we can see on these figures the location identification of $g3$ is very accurate in the two cases with a maximum deviation of 0.8 mm. This is not the case with $g5$ identification. In Fig. 12 three sources are around $g5$ within a distance d of 8.7 mm. The sum of their intensities is equal to 40.9 W m^{-1}, which is close to the real value of $g5$ (40 W m^{-1}). The results presented in Fig. 13 are similar to those presented in Fig. 11, with two sources close to $g3$ and $g5$ and the others with a small strength. The values of standard deviation and Euclidean norms obtained with the two solutions are of the same order of magnitude. In this case, the correct solution cannot be determined and the use of one or more thermocouples would be necessary to eliminate the wrong solution.

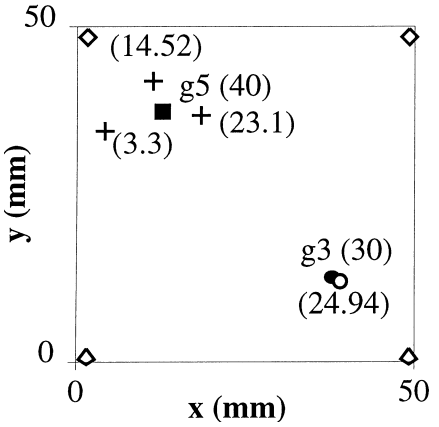

Fig. 12. Two sources activated, $g3$ and $g5$, four declared, initial locations at the four corners (◇), $\|\hat{\Theta} - \tilde{\Theta}\| = 0.86°C$, $\sigma(\theta) = 0.12°C$.

4. Conclusion

In this paper, we have presented our approach for multiple-point heat sources identification in the steady case. The results of the method combining the location and strength identification are satisfactory considering the presented experimental results. These results obtained on a 2D diffusive system show that a set of point heat sources can be identified by using infrared thermography only, without any thermocouple. The transient case can be treated using a similar approach, with for example the identification of sources moving in space during the experiment.

References

[1] C. Le Niliot, The boundary element method for the time varying strength estimation of point heat sources: application to a two-dimensional diffusion system, Numer. Heat Transfer, Part B 33 (1998) 301–321.

[2] A.J. Silva Neto, M.N. Ozisik, Two-dimensional inverse heat conduction problem of estimating the time-varying

strength of a line heat source, J. Appl. Phys. 71 (11) (1992) 5357–5362.
[3] C. Yang, The determination of two heat sources in an inverse heat conduction problem, Int. J. Heat Mass Transfer 42 (1999) 345–356.
[4] C. Le Niliot, F. Rigollet, D. Petit, An experimental identification of line heat sources in a diffusive system using the boundary element method, Int. J. Heat Mass Transfer 43 (2000) 2205–2220.
[5] M.N. Ozisik, Heat Conduction, second ed., Wiley, New York, 1993.
[6] J. Hadamard, Le Problème de Cauchy et les Équations Aux Dérivées Partielles Linéaires Hyperboliques, Hermann, Paris, 1932.
[7] C.A. Brebbia, J.C.F. Telles, L.C. Wrobel, Boundary Element Techniques, Springer, Berlin, 1984.
[8] C. Le Niliot, Méthode des éléments de frontière pour la résolution des problèmes inverses en diffusion thermique, University doctoral thesis, Université de Provence, Marseille, France, 1991.
[9] R. Pasquetti, C. Le Niliot, Conduction inverse par éléments de frontière: cas stationnaire, Rev. Phys. Appl. 25 (1990) 99–107.
[10] J.V. Beck, B. Blackwell, C.R.St. Clair, Inverse Heat Conduction, Ill-Posed Problems, Wiley Interscience, New York, 1985.
[11] M. Banaszkiewicz, K. Seiferlin, T. Spohn, G. Kargl, N. Kömle, A new method for the determination of thermal conductivity and thermal diffusivity from linear heat source measurements, Rev. Sci. Instr. 68 (11) (1997) 4184–4190.
[12] F. Papini, P. Gallet, Thermographie Infrarouge: Image et Mesure, Masson, Paris, 1994.
[13] W.H. Mc Adams, Heat Transmission, third ed., McGraw-Hill Kogakusha, Tokyo, 1954.